

# New or missing energy

Franzosi, Diogo Buarque; Frandsen, Mads Toudal; Shoemaker, Ian M.

*Published in:*
Physical Review D (Particles, Fields, Gravitation and Cosmology)

*DOI:*
10.1103/PhysRevD.93.095001

*Publication date:*
2016

*Document version*
Final published version

*Citation for pulished version (APA):*
Franzosi, D. B., Frandsen, M. T., & Shoemaker, I. M. (2016). New or missing energy: Discriminating Dark Matter from Neutrino Interactions at the LHC. Physical Review D (Particles, Fields, Gravitation and Cosmology), 93(9), 095001-1-095001-10. [095001]. DOI: 10.1103/PhysRevD.93.095001

PHYSICAL REVIEW D **93,** 095001 (2016)

# New or $\nu$ missing energy: Discriminating dark matter from neutrino interactions at the LHC

Diogo Buarque Franzosi,* Mads T. Frandsen,† and Ian M. Shoemaker‡

*CP$^3$-Origins and Danish Institute for Advanced Study, Danish IAS, University of Southern Denmark, Campusvej 55, DK-5230 Odense M, Denmark*

(Received 9 February 2016; published 3 May 2016)

Missing energy signals such as monojets are a possible signature of dark matter (DM) at colliders. However, neutrino interactions beyond the Standard Model may also produce missing energy signals. In order to conclude that new "missing particles" are observed, the hypothesis of beyond the Standard Model neutrino interactions must be rejected. In this paper, we first derive new limits on these nonstandard neutrino interactions (NSIs) from LHC monojet data. For heavy NSI mediators, these limits are much stronger than those coming from traditional low-energy $\nu$ scattering or $\nu$ oscillation experiments for some flavor structures. Monojet data alone can be used to infer the mass of the missing particle from the shape of the missing energy distribution. In particular, 13 TeV LHC data will have sensitivity to DM masses greater than $\sim$1 TeV. In addition to the monojet channel, NSI can be probed in multilepton searches which we find to yield stronger limits at heavy mediator masses. The sensitivity offered by these multilepton channels provides a method to reject or confirm the DM hypothesis in missing energy searches.

DOI: 10.1103/PhysRevD.93.095001

## I. INTRODUCTION

Missing energy signals are the telltale clue of the production of stable neutral objects. Indeed the imbalance of momentum and energy is in fact precisely the way in which the neutrino was first discovered. Supposing that the LHC finds anomalous "missing energy" events above Standard Model (SM) backgrounds, the determination of their origin will be of paramount importance. As known sources of missing energy, a plausible origin of new missing energy data will be neutrinos. However, new neutral particles beyond the Standard Model (BSM) such as dark matter can also produce missing energy signals at colliders.

In this paper we explore how LHC data can be used to distinguish these two potential sources of missing energy. We illustrate that both the DM mass and the $SU(2)$ charge of neutrinos can be used to discriminate between singlet dark matter (DM) and SM neutrinos.[1] For simplicity we will focus on the so-called "monojet" signature in which a single hard jet recoils against "nothing" [2–30]. Previous work in this direction using Tevatron and early LHC data was carried out in Ref. [11].

We begin by reviewing current experimental limits on neutrino-proton interactions in the context of effective field theory. Up to dimension 6, we can have

(i) Neutrino magnetic dipole moments:

$$\mathcal{L} \supset \mu_\nu F^{\mu\nu} \bar{\nu} \sigma_{\mu\nu} \nu, \tag{1}$$

where the spin matrix is $\sigma_{\mu\nu} \equiv i[\gamma_\mu, \gamma_\nu]/2$ and $\mu_\nu$ is the magnetic moment [measured in units of the Bohr magneton $\mu_B \equiv e/(2m_e)$, where $e, m_e$ are the charge and mass of the electron].

(ii) Nonstandard neutrino interactions (NSIs):

$$\mathcal{L}_{\rm NSI} = -2\sqrt{2} G_F \varepsilon^{fP}_{\alpha\beta} (\bar{\nu}_\alpha \gamma_\rho \nu_\beta)(\bar{f} \gamma^\rho P f), \tag{2}$$

where the matrix $\varepsilon^{fP}_{\alpha\beta}$ specifies the strength of the $\nu$-$f$ interaction, in units of Fermi's constant, $G_F \equiv 1/\sqrt{2} v_{\rm EW}^2 \simeq 1.2 \times 10^{-5}$ GeV$^{-2}$, with $v_{\rm EW} = 246$ GeV. The labels $\alpha, \beta$ are flavor indices running over $e, \mu, \tau$, and $P$ is a projection operator. We take $f$ to be any SM fermion (though only the *vector* components of $f = e, u, d$ are relevant for neutrino oscillations).

Let us first consider whether neutrino magnetic moments below current limits can produce sizeable missing energy at the LHC. For Majorana neutrinos the $3 \times 3$ matrix $\mu_\nu$ does not have diagonal entries and is antisymmetric but is completely general if they are instead Dirac. In the SM the magnetic moment is proportional to the neutrino mass and therefore extremely small, $\mu_\nu^{\rm SM} \sim 10^{-20}\ \mu_B$. For Dirac neutrinos in BSM scenarios, naturalness considerations on the coefficients of effective operators imply $\mu_\nu \lesssim 10^{-14}\ \mu_B$ [31], far below present experimental sensitivity. Finally for Majorana neutrinos reactor data as measured by the GEMMA spectrometer constrains, $\mu_\nu < 3.2 \times 10^{-11}\, \mu_B$ [32], while the 7 TeV LHC sensitivity is around $\sim 3 \times 10^{-5}\ \mu_B$ [33], far above what is

*franzosi@cp3-origins.net
†frandsen@cp3-origins.net
‡shoemaker@cp3.dias.sdu.dk

[1]If DM itself transforms nontrivially under $SU(2)$, the situation is more complex. We leave for future work a systematic study in this direction but note that some of the implications of $SU(2)$ charged DM in a variety of representations have been studied in, e.g., Ref. [1].

 

allowed by reactor and solar data [34]. We conclude that neutrino magnetic moments will not produce sizeable missing energy at the LHC.

Proceeding now to operators of mass dimension 6, we turn our attention to the NSI operators between quarks and neutrinos. NSIs were first introduced in 1977 [35] and continue to be of wide phenomenological interest [11,36–48] (see Refs. [36,49,50] for reviews).

They are constrained by solar [37,51–57], atmospheric [38,39,46,58–61], long-baseline [41–43,45,48,61,62], collider [11,44,47,63], cosmological [64], and neutrino scattering data [36,40,49].

One may worry that sizeable NSIs would also induce large charged lepton interactions [36,65,66]. Indeed, to evade the very strong limits from the charged lepton equivalent of Eq. (2), we consider dimension-8 operators of the form [63]

$$\mathcal{L}_{\rm NSI}^{\rm dim-8} = -\frac{4\epsilon_{\alpha\beta}^{fP}}{v_{\rm EW}^4}(\overline{HL_\alpha}\gamma_\mu HL_\beta)(\bar{q}\gamma_\mu q), \tag{3}$$

where $H$ is the SM Higgs doublet. In a unitary gauge and upon electroweak (EW) symmetry breaking, we can make the replacement $H \to (h + v_{\rm EW})/\sqrt{2}$. Thus, at low energies, one indeed generates Eq. (2) without charged lepton interactions of the same strength.

The remainder of this paper is organized as follows. First we introduce our simplified model and calculational framework in Sec. II. In Sec. III we derive new constraints on NSIs based on the latest monojet data from the LHC. Then we turn to projections of monojet sensitivity at 13 TeV and the ability to infer the mass of the missing particles from the shape of the $E_T$ distribution. We find that for contact interactions, DM masses $\gtrsim$700 GeV can be discriminated from NSI with about 100 fb$^{-1}$ of integrated luminosity. In Sec. IV we then use two distinct multilepton channels to probe NSI. These searches have neutrino flavor dependent sensitivity and have better sensitivity than monojets for heavy mediators of NSI. In Sec. V we discuss the complementarity of these channels along with low-energy probes of NSI for DM-neutrino discrimination and conclude in Sec. VI.

## II. MODEL AND CALCULATIONAL FRAMEWORK

In order to derive LHC limits on NSI/DM couplings $\epsilon$, we have implemented two models in the Universal FeynRules Format (UFO) [67] by adding to the SM a spin-1 mediator, $V^\mu$, which interacts with neutrinos, quarks, and DM $X$ through the phenomenological Lagrangians:

$$\begin{aligned}\mathcal{L}_{\rm NSI} &= g_\nu(\bar{\nu}P_L\gamma_\mu\nu)V^\mu + (\bar{q}\gamma_\mu(g_q^V + g_q^A\gamma^5)q)V^\mu,\\ \mathcal{L}_{\rm DM} &= g_X(\bar{X}\gamma_\mu X)V^\mu + (\bar{q}\gamma_\mu(g_q^V + g_q^A\gamma^5)q)V^\mu,\\ &\quad + m_X\bar{X}X,\end{aligned} \tag{4}$$

where $\nu$ and $q$ are summed over all neutrino and quark flavors, respectively, and $m_X$ is the DM mass. The Lagrangian $\mathcal{L}_{\rm NSI}$ correctly reproduces the contact interaction, Eq. (2), when the vector mass $m_R$ is large compared to the center-of-mass energy. Note that the DM literature tends to report limits on the scale of the dimension-6 operator, $\Lambda$, defined as $(\bar{X}\gamma_\mu X)(q\gamma^\mu q)/\Lambda^2$. The conversion from $\Lambda$ to the NSI $\epsilon$ parameter in this context is $\epsilon = (2G_F\Lambda^2)^{-1}$.

The main aim of this paper is to illustrate how $\mathcal{L}_{\rm NSI}$ can be discriminated from $\mathcal{L}_{\rm DM}$ and gauge the relevant parametric dependencies present in $s$-channel completions of NSI ($t$-channel completions are very strongly constrained [11,47] and not considered further). For details on a more complete $Z'$ model, we refer the reader to Refs. [56,68–70] for additional models. Furthermore, it is important to highlight that a complete model typically produces signatures *in addition* to the monojet and multilepton channels we consider here, making our approach conservative.

Simplified models of the type in Eq. (4) have been studied extensively in the DM literature [7,9,10,12,13,17,29,71–81]. While dijet searches provide additional constraints on the models considered here (see, e.g., Refs. [13,29]), both $\mathcal{L}_{\rm NSI}$ and $\mathcal{L}_{\rm DM}$ contribute equally to this channel, and thus it is not a useful discriminatory tool.

Our calculational framework is as follows. To keep the analysis simple, we consider only vector couplings, i.e., $g_q^A = g_X^A = 0$. We import the UFO model into the `MadGraph5_aMC@NLO` framework [82], where helicity amplitudes are generated by the `ALOHA` [83] code. The hard scattering simulation is then processed through parton showering and hadronization using `Pythia 6` [84] and `Pythia 8` [85]. Finally we perform a fast detector simulation for the monojet analysis, using both the PGS [86] and DELPHES [87] programs to check our results.

For the monojet computation, we use the CTEQ 6L1 [88] set of parton distribution functions (PDF), as this is used by the experimental collaboration, and NNPDF 2.3 [89] for the other processes. We chose the default dynamical factorization and renormalization scales of `MadGraph_aMC@NLO`.

## III. MONOJET SEARCHES

Any long-lived or stable neutral states, such as neutrinos and DM, with couplings to protons can lead to monojet events at the LHC. These monojet processes, depicted in Fig. 1 (left), are characterized by large missing transverse energy and a very hard jet. In Ref. [90], the CMS experiment searched for monojets with $\sqrt{s} = 8$ TeV in the center-of-mass energy and $\mathcal{L} = 19.5$ fb$^{-1}$ of integrated luminosity, reporting an upper limit at 90% C.L. of $\epsilon = 0.053$ for a vector operator and an invisible particle mass $m_X = 1$ GeV.

To estimate the NSI signal, we compute the cross sections for the hard scattering process,

$$pp \to V \to \bar{\nu}\nu + 1, 2j, \tag{5}$$

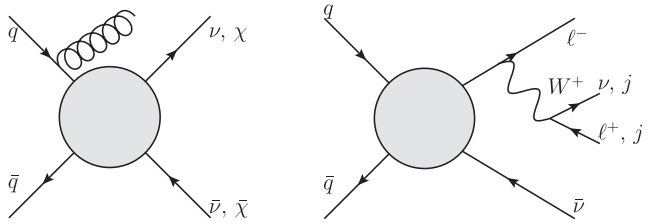


FIG. 1. Typical Feynman diagrams for $pp \to \bar{\nu}\nu(\bar{X}X) + j$ (*left panel*) and $pp \to \bar{\nu}\nu \to \ell^{\mp} + W^{\pm} + \bar{\nu}$ (*right panel*). Though singlet DM and neutrinos are largely degenerate in the former process, only SM neutrinos give rise to the latter process.

with one and two jets (quarks or gluons), $j$, using the framework described in Sec. II. In particular we use the M. L. Mangano prescription [91] for matching matrix elements with soft jets from the parton shower. Following the CMS analysis [90], we require the leading jet to have $p_T(j) > 110$ GeV and to be in the central region of the detector $|\eta(j)| < 2.6$. Events with more than three jets with $p_T > 30$ GeV and $|\eta| < 4.5$ are discarded, while a second jet is allowed as long as the difference in the azimuthal angle to the leading jet is less than 2.5, $\Delta\phi(j_1, j_2) < 2.5$. We further require the missing transverse energy $E_T > 450$ GeV, found to give the best discriminant.

With this analysis setup, we found excellent agreement in the shape of the missing transverse energy distribution for $Z(\nu\nu) + \text{jets}$ and $W(\ell\nu) + \text{jets}$ SM background. We also found agreement within scale and PDF uncertainties for the number of events. We nevertheless use the fact that the collaboration provides a more precise prediction from data driven techniques, and we rescale our predictions by a correction factor of 1.19 to agree with their prediction.

The CMS Collaboration report 157 events as the upper 95% C.L. limit on the number of events from new physics. Note that a downward fluctuation in the observed number of events gives a constraint about 30% stronger than expected. We compute the resulting NSI limits that are shown in Fig. 2, as a function of the mediator mass and width ($\Gamma_V = \frac{m_V}{3}, \frac{m_V}{10}, \frac{m_V}{8\pi}$).

Note that *flavor diagonal* NSIs interfere with the dominant SM background process, $pp \to Z + j \to \bar{\nu}\nu + \text{jets}$. The strength of the effect depends on the Lorentz structure of the coupling and the mass of the mediator. The effect is small in the contact interaction limit, $\lesssim 5\%$, but can be as large as 20% when the mass of the mediator is close to the $Z$ mass. This depends too on the flavor of the quarks, since they carry different $SU(2)$ and hypercharges. The overall effect can be seen in the dependence in $\theta$ of the upper limits on $\epsilon$, shown in Fig. 3, where $\theta$ is defined as the direction of the coupling in the $(V, A)$ space, i.e., $\varepsilon^P = \varepsilon(\sin(\theta) + \cos(\theta)\gamma^5)$. Although interference is a feature specific to the NSI case, it only affects the total number of events and does not aid in distinguishing between dark matter and NSI. We shall therefore omit it in the following.

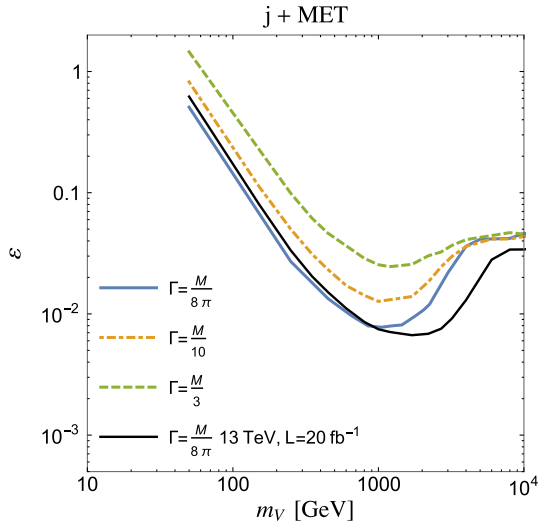


FIG. 2. Here we display the CMS monojet limits [90] on NSI at 95% C.L. for three different choices of the mediator width at $\sqrt{s} = 8$ TeV and with integrated luminosity $\mathcal{L} = 19.5$ fb$^{-1}$. The black solid line denotes the expected limit at 95% C.L. with $\sqrt{s} = 13$ TeV and $L = 20$ fb$^{-1}$.

### A. Projection to $\sqrt{s} = 13$ TeV LHC and jet $p_T$ shape analysis

The next LHC run at $\sqrt{s} = 13$ TeV will either further limit or discover NSI and/or DM in monojet searches. In Fig. 2 we show our projected LHC monojet 95% C.L. limit as the solid black line for $m_X = 0$ GeV at $\sqrt{s} = 13$ TeV with the luminosity $\mathcal{L} = 20$ fb$^{-1}$ as expected for the first year of collisions. We use the same setup used at $\sqrt{s} = 8$ TeV and the same normalization rescaling. We assume a systematic error of 5% and perform a $\chi^2$ analysis with which the expected bounds at 8 TeV quoted by CMS were reproduced within error. At this luminosity the systematic error dominates, and increasing the luminosity further does not appreciably change the experimental sensitivity.

The first observable we use to distinguish NSI from DM is the monojet $E_T$ distribution. Sufficiently heavy DM masses are kinematically relevant at LHC energies and affect the shape of the $E_T$ distribution.

The allowed value of $\varepsilon$ just below the 95% C.L. present limit is ~0.04 in the contact interaction limit, for massless missing energy particles. This situation, i.e., $\varepsilon = 0.04$, would produce a $2.9\sigma$ excess according to our projections for the first year Run II of the LHC. The same excess of events can be produced for lower $\varepsilon$ but lighter mediator mass or larger $\varepsilon$ and heavier particles in the final state.

In Fig. 4 we show the $E_T$ distribution for $L = 100$ fb$^{-1}$ for DM masses, $m_X = 500$, 700, 1000 GeV. We do not display lighter DM masses since these are effectively indistinguishable from the massless case (as can be seen in Fig. 4). The total cross sections are all normalized to the $\varepsilon = 0.04$ massless case (shown in the projection Fig. 5) so that all signals produce the same total number of events

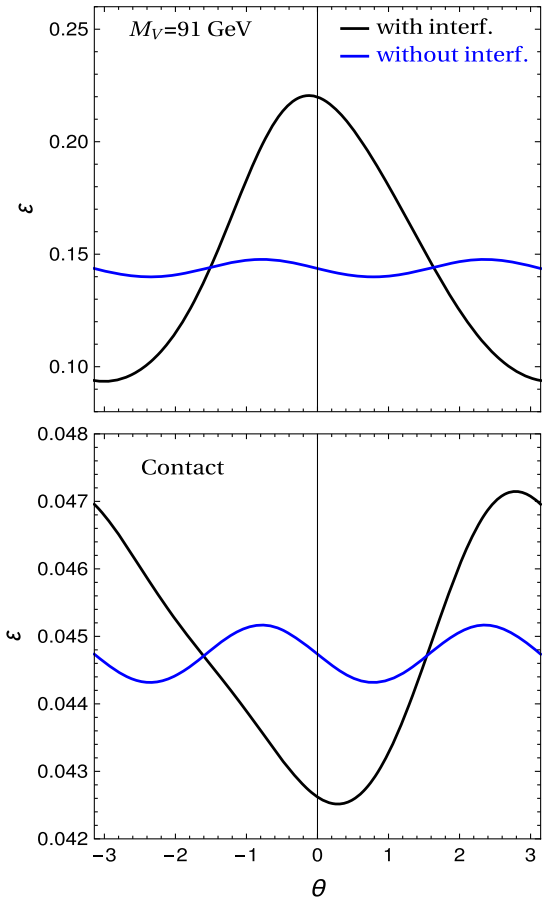


FIG. 3. Interference and dependence on the Lorentz nature of the interaction. The interference is included in the black curve and absent in the blue one. In the upper panel, the mediator mass is $m_V = 91$ GeV [with width $\Gamma = m_V/(8\pi)$], while the lower panel refers to the contact limit.

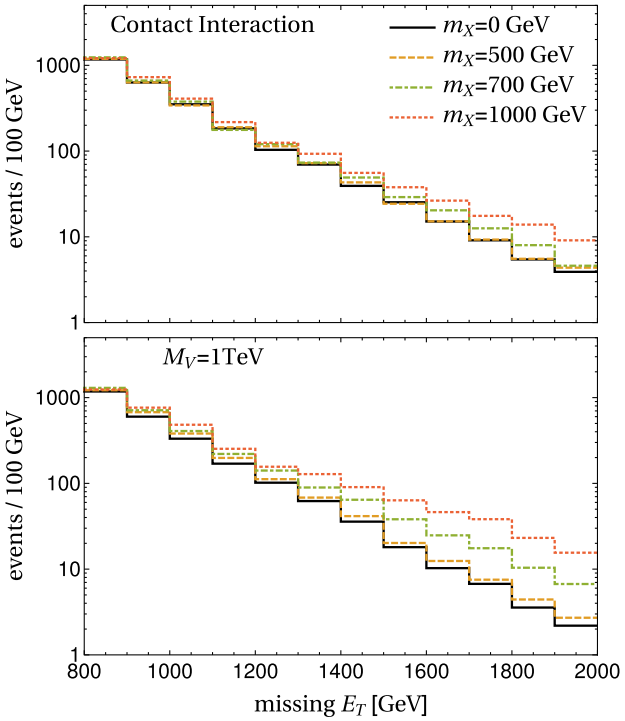


FIG. 4. Distribution of events in missing transverse energy, $\not{E}_T$, for $\sqrt{s} = 13$ TeV and $\mathcal{L} = 100$ fb$^{-1}$ for DM masses $m_X = 0$ GeV, 500 GeV, 700 GeV, and 1 TeV. Here each distribution is normalized to produce the same number of events as in the contact interaction limit, with $m_X = 0$, and $\varepsilon = 0.04$, which corresponds to the signal strength just below the present bounds (see, e.g., Fig. 2). *Upper panel:* contact interaction. *Lower panel:* mediator mass $m_V = 1$ TeV.

with $\not{E}_T > 450$ GeV. In the upper panel, we show the contact interaction case. In the lower panel, we show the equivalent prediction for a mediator mass $m_V = 1$ TeV, also keeping the same total number of events with $\not{E}_T > 450$ GeV as the $\varepsilon = 0.04$ massless case in the contact interaction limit. The corresponding value of $\varepsilon$ is $\varepsilon \sim 0.0068$. A much harder distribution can be noticed.

The shape of the $\not{E}_T$ distributions clearly allows us to distinguish between the heaviest and lightest DM masses. We quantify this in a simple $\chi^2$ analysis. In addition to the statistical error, we assume a systematic error per bin of 5% for the background and 20% for the dark matter contribution, as reported in Ref. [90]. The $\chi^2$ distribution is then given by

$$\chi^2[m_X; 0\ \text{GeV}] = \sum_i \left[\frac{S_i(m_X) - S_i(0\ \text{GeV})}{\sigma_i}\right]^2, \qquad (6)$$

where $S_i(m_X)$ is the number of events in the $i$th bin. The distribution is shown in Fig. 6 as a function of the integrated

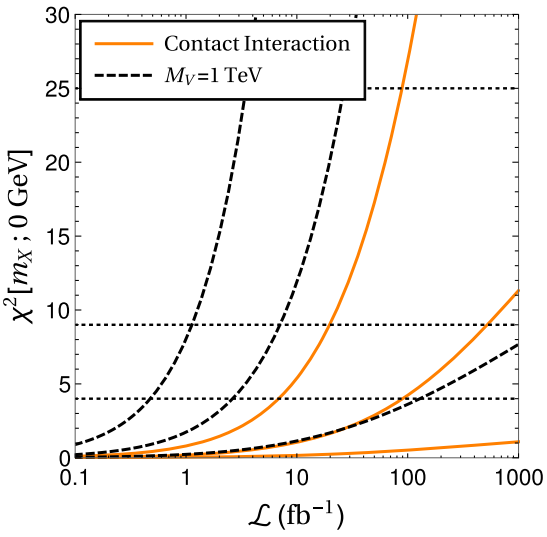


FIG. 5. $\chi^2$ projection analysis. Here we generate events at $\sqrt{s} = 13$ TeV in a model with contact interactions (orange solid line) and for mediator mass $m_V = 1$ TeV (black dashed line) just below present bounds with a 0 GeV DM mass. The $\chi^2[m_X; 0\ \text{GeV}]$ is computed by fitting $m_X = 500, 700, 1000$ GeV DM masses (lowest to highest curves) to the input data from a massless invisible particle. The $3\sigma$, $4\sigma$, and $5\sigma$ confidence levels are plotted for reference.

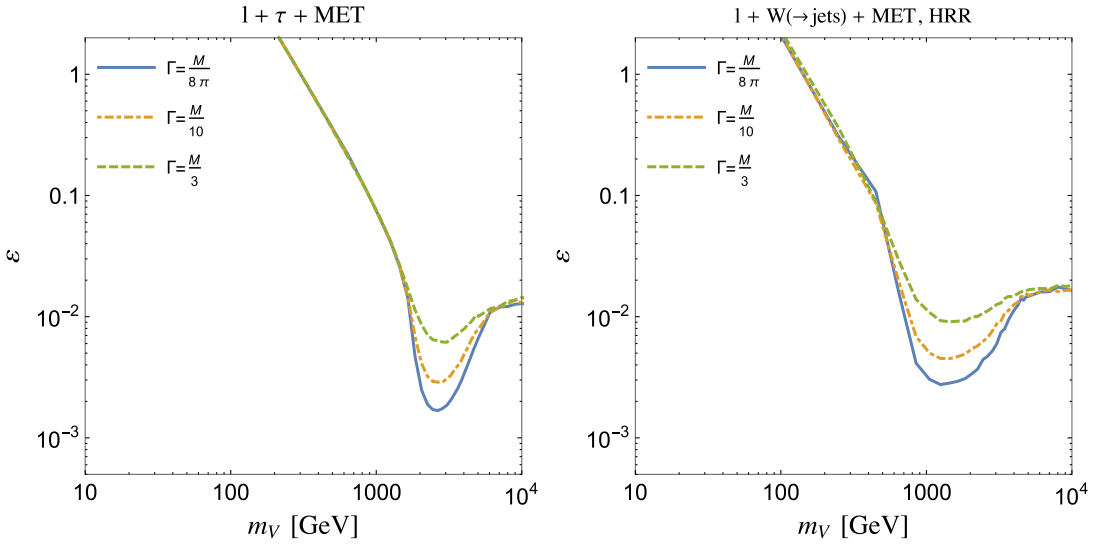


FIG. 6. Each panel displaying individual LHC search limits on NSI for three different choices of the mediator width. The left panel displays the $\tau + \ell +$ MET search from ATLAS [92], while the right panel shows the sensitivity from the $jj + \ell +$ MET search from ATLAS [93] (see the text for details).

luminosity at the $\sqrt{s} = 13$ TeV LHC run for the three masses $m_X = 500$, 700, 1000 (from the lower curve to the highest one). In the case of a low mass mediator, $m_V = 1$ TeV (dashed black line), it will be easier to distinguish a massive final state from neutrinos, while in the contact interaction case (solid orange line), the missing energy distributions are more alike.

Note that the effective operator description will break down if $2m_X > m_V$ since in this case the momentum flowing through the vector propagator is necessarily larger than its mass. We have been careful to choose the vector mass in the contact case such that this condition is always satisfied and the contact description should be sufficiently accurate. Note that the contact-level monojet limits translate to a bound of $\Lambda \gtrsim 1$ TeV, though we stress that these limits are still applicable to TeV-scale mediators with large couplings.

## IV. MULTILEPTON SEARCHES

In addition to the monojet signal, NSI can produce signals in other channels due to the $SU(2)$ charge of neutrinos. For example, as shown in Fig. 1 one of the produced neutrinos can radiate a $W$-boson that decays to either jets or $\ell + \nu$,

$$pp \to \bar{\nu}\nu \to \bar{\nu} + W^{\pm}\ell^{\mp}. \tag{7}$$

Mutlilepton searches of this type have been used previously to constrain NSI using LHC data [11,44].

In order to exclude the NSI hypothesis and claim the discovery of a new source of missing energy, we must exclude all possible neutrino flavor structures of NSI. For this it is necessary to consider the lepton in the final state to be a tau, a muon, or an electron. Since the mixed flavor interaction, e.g., $\varepsilon_{\tau\mu}, \varepsilon_{e\mu}$, will regardless produce one of these leptons, this condition is also sufficient to constrain mixed terms. For the muon and electron in the final state, we have relied on the $\sqrt{s} = 8$ TeV and $\mathcal{L} = 20.3$ fb$^{-1}$ ATLAS search for resonant diboson production where one boson decays leptonically and the other hadronically [93]. For the tau lepton final state, we have used the ATLAS search for supersymmetry with large missing transverse energy, jets, and at least one tau lepton, at $\sqrt{s} = 8$ TeV and $\mathcal{L} = 20.3$ fb$^{-1}$ of data [92]. We will briefly describe each analysis and the results in the following.

The searches we used are not optimized for the NSI signal topologies, and we expect that dedicated analyses can improve our results. Moreover NSI can lead to signals not considered here, but they are expected to be subdominant. For example $pp \to \nu\nu(Z \to jj/\ell^+\ell^-)$, where the neutrino radiates a $Z$-boson, will suffer from large background from Drell-Yan production. Similarly in $pp \to \nu\ell(W \to \ell\nu)$ with highly energetic $\ell^+\ell^-$ system, the $W$ cannot be reconstructed, suffering from many more backgrounds. Nonetheless, all these channels may contribute to put bounds on NSI and require a dedicated analysis.

We begin by considering hadronic decays of the $W$s.

### A. $pp \to \bar{\nu} + W^{\pm}\ell^{\mp}$, $W^{\pm} \to jj$, $\ell = e, \mu$

In this analysis the $W$-boson is required to be highly boosted to reduce hadronic backgrounds. Consequently the two jets from the $W$ are likely to appear as a single jet making jet substructure techniques relevant. The parton-level computation was passed through parton showering and hadronization using `Pythia 8`.

We employ the event selection of the experimental analysis in Ref. [93]: leptons are required to have transverse momentum $p_T > 25$ GeV and $|\eta| < 2.5$. Moreover they are required to satisfy the following isolation criteria: the scalar sum of $p_T$ of tracks with $p_T > 1$ GeV within $\Delta R = \sqrt{\Delta\eta^2 + \Delta\phi^2} = 0.2$ of the lepton track is required to be less than 15% of the lepton $p_T$. The missing transverse energy, defined as the negative of the vectorial sum of the transverse momenta of all electrons, muons, and jets within $|\eta| < 4.9$, is required to be $\not{E}_T > 30$ GeV.

We cluster the jets with two different jet definitions provided by `Fastjet 3.1.2` [94]. For the signal region where the $W$ has large $p_T$ and the jets cluster into a single "fat" jet, we use the Cambridge algorithm. Otherwise, we use the anti-$k_T$ algorithm with $R = 0.4$. The ATLAS analysis [93] defines three signal regions as the merged region (MR), the high-$p_T$ resolved region (HRR), and the low-$p_T$ resolved region (LRR), respectively. In the MR the largest $p_T$ jet $(J)$ is taken to represent a decayed $W$-boson, if it fulfills $p_T(J) > 400$ GeV, $|\eta(J)| < 2$, and $65\ \text{GeV} < m(J) < 105$ GeV with the azimuthal angle difference between $J$ and $\vec{\not{E}}_T$ satisfying $\Delta\phi(J, \not{E}_T) < 1$. Additionally, the $p_T$ of the lepton and $\not{E}_T$ system is required to be $p_T(\ell\not{E}_T) > 400$ GeV.

If the event does not pass these cuts, we proceed to the resolved region, where the two leading 0.4 anti-$k_T$ jets, $j_{1,2}$, reconstruct a decayed $W$-boson if $|\eta(j)| < 2.8$, $65\ \text{GeV} < m(jj) < 105$ GeV, and $\Delta\phi(j_1, \not{E}_T) < 1$. The HRR (LRR) is defined by $p_T(jj) > 300(100)\,\text{GeV}$, $p_T(j) > 80(30)\,\text{GeV}$, and $p_T(\ell\not{E}_T) > 300(100)$ GeV.

After normalizing with an approximate next-to-leading-order K-factor of K = 1.7 [95], we get reasonable agreement in all three regions for the number of events expected from the SM diboson background. Therefore we assume that this simple analysis is accurate enough for our needs.

We used the model described by Eq. (4) to estimate the visible cross sections, $\sigma_S$, and associated number of events, $S = \sigma_S\mathcal{L}$, of the NSI signal, where the luminosity is $\mathcal{L} = 20.3\ \text{fb}^{-1}$. We rescale our prediction by a K-factor $K = 1.2$ to account for QCD corrections extracted from on-shell $Z'$ production [96]. We moreover assumed a conservative flat theoretical error of 30% to account for PDF and scale uncertainty. The SM prediction for the total number of events and uncertainty, $B \pm \sigma_B$, is $161500 \pm 2300$, $870 \pm 40$, and $295 \pm 22$ for LRR, HRR, and MR, respectively and the observed number of events, $N^{\text{obs}} = 157837$, 801, and 295, respectively. We summed the errors in quadrature, $\sigma^2_{\text{TOT}} = \sigma^2_B + S + (0.3S)^2$, and estimated the 95% C.L. upper limit on $S$ using a $\chi^2$ analysis, solving for $S$ the equation

$$\left(\frac{S + B - N^{\text{obs}}}{\sigma_{\text{TOT}}}\right)^2 = \chi^2_{.05}(\text{d.o.f.} = 1) = 3.84. \quad (8)$$

The resulting limits in terms of $\varepsilon$ are shown in Fig. 7.

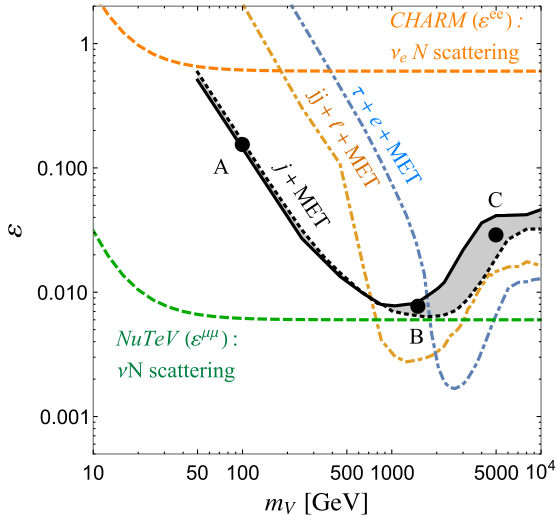


FIG. 7. In the mediator mass-coupling plane $(m_V, \varepsilon)$, we compare existing searches for NSI from neutrino-nucleus scattering to the LHC monojet limits derived in this paper. The upper curve in the gray band depicts the current monojet limits, while the lower curve shows the 13 TeV projection with 100 $\text{fb}^{-1}$. The dot-dashed curves represent the current multilepton constraints on NSI based on 8 TeV LHC data. Additional low-energy constraints on the NSI parameter $\varepsilon_{\alpha\beta}$ include NuTeV's constraint on $\varepsilon_{\mu\mu}$ [97] and CHARM's constraint on $\varepsilon_{ee}$ [98]. For reference the constraint on $\varepsilon_{\tau\tau}$ is sufficiently weak that it does not appear on the plot (see Ref. [36]).

Next we will consider leptonically decaying $W$-bosons.

### B. $pp \to \bar{\nu} + W^{\pm}\tau^{\mp}$, $W^{\pm} \to \ell\nu$ and $pp \to \bar{\nu} + W^{\pm}\ell^{\mp}$, $W^{\pm} \to \tau\nu$, $\tau \to$ hadrons, $\ell = e, \mu$

The signal region defined in the ATLAS search [92] relevant for our final state is referred to as the $\tau +$ lepton "gauge-mediated supersymmetry breaking signal" region, which requires a reconstructed hadronically decayed tau lepton and a single isolated electron or muon. Nonstandard neutrino interactions involving a tau lepton will contribute to this process, but other NSI flavor structures without a tau lepton will equally contribute when the $W$-boson decays to a tau lepton and tau neutrino.

In our analysis we assume the tau is reconstructed with 70% of efficiency in this region, as reported in the analysis. In addition we reproduce the kinematical cuts given therein: $p_T(\ell) > 25$ GeV; $p_T(\tau) > 20$ GeV; lepton transverse mass, $m_T(\ell) > 100$ GeV, defined by

$$m_T(\ell) = \sqrt{2p_T(\ell)\not{E}_T(1 - \cos(\Delta\phi(\ell, \not{E}_T)))}; \quad (9)$$

and $m_{\text{eff}} > 1700$ GeV, where

$$m_{\text{eff}} = p_T(\ell) + p_T(\tau) + \not{E}_T. \quad (10)$$

The 95% C.L. limit on the visible cross section provided by the ATLAS Collaboration is 0.20 fb for the $\tau + e$ channel and 0.26 fb for the $\tau + \mu$ channel. Using these numbers we find the 95% C.L. exclusion limit shown in

Fig. 7 as the blue dot-dashed line. The limit shown is for NSI involving a tau lepton, $\epsilon_{\tau\tau}$; however the difference with respect to other flavor structures is small. For $\epsilon_{ee}$ it is only a few percent, and for $\epsilon_{\mu\mu}$ it is about 15% due to the weaker experimental upper limit on the muon channel.

## V. DISCUSSION

After deriving new limits on NSI, we finally assess what future LHC data can unveil. If anomalous missing energy events appear in the next run of the LHC, they will be consistent with either DM or NSI just at the border of the current constraints. If the events are due to TeV scale DM, then $\not{E}_T$ shape analysis will be enough to rule out NSIs as the origin. If that is not the case, then we can still use multilepton channels to help discriminate between NSIs and DM. To illustrate this point, we consider three distinct benchmark scenarios:

(i) *Benchmark A*, $(m_V, \varepsilon) = (100\ \text{GeV}, 0.15)$: The LHC is not a particularly good environment for discriminating neutrinos from DM in the light mediator limit. Although NuTeV's constraint [97] on $\mu$-flavored diagonal NSI shown as the orange dashed line in Fig. 7 allows us to conclude that this particular flavor structure is not responsible for anomalous missing energy events, the other flavor structures have much weaker constraints and cannot be excluded as potential explanations of LHC monojet signals. NSI with $\tau$ or $e$ flavored interactions can simultaneously escape low-energy probes and multilepton searches at the LHC. Future data from dedicated low-energy experiments searching for $\nu_e - N$ or $\nu_\tau - N$ may help resolving this.

(ii) *Benchmark B*, $(m_V, \varepsilon) = (1500\ \text{GeV}, 8 \times 10^{-3})$: Here the LHC's ability to discriminate NSI from the DM hypothesis is much more favorable given the strength of $e$, $\mu$ flavored NSI limits. Thus, although monojet data will be at the discovery level, $\tau$-flavored NSI cannot be discriminated at the LHC from a DM interpretation. However, since the $\tau + e + \text{MET}$ search utilized in the present paper is not optimized for NSI, it is possible that a dedicated analysis could help resolve this.

(iii) *Benchmark C*, $(m_V, \varepsilon) = (5\ \text{TeV}, 0.03)$: This final benchmark is the most optimistic, as the discrimination between NSI and DM is robust. This is because there are two sensitive probes of NSI since both the $\tau + e + \text{MET}$ and $jj + \ell + \text{MET}$ channels yield stronger constraints than monojets. Thus, for example, monojet data originating from this benchmark would already be excluded from being of NSI origin with present multilepton data.

Summarizing, the multilepton probes are crucial for distinguishing between DM and NSIs in benchmark C and partially in the case of benchmark B. For benchmark A input from additional low-energy experiments will be needed. These can be either DM or neutrino probes. For example, DM direct detection data can be used to determine the mass of the DM and bound the mediator mass [99–101].

Alternatively in the case of neutrinos, constraints on neutrino scattering will improve shortly. Using the methods outlined in Ref. [40], the COHERENT [102,103] Collaboration's multitarget measurement of coherent elastic neutrino-nucleus scattering can be used to substantially strengthen the limits on NSI [102] from NuTeV [97] and CHARM [98].

Finally, thanks to the modification of neutrino oscillation probabilities that (vector) NSI induces, long-baseline and solar neutrino data will also further limit NSI. Future probes of NSI include long-baseline experiments such as NO$\nu$A and DUNE [45] as well as atmospheric data from IceCube DeepCore [46] and solar neutrino data from DM direct detection experiments [104].

These complementary experimental searches will be tremendously useful in obtaining better sensitivity to NSI.

## VI. CONCLUSION

If anomalous events with missing energy are found in the next run of the LHC, determining the nature of the missing particles will be of utmost importance. Given that neutrinos are the only confirmed source of missing energy to date, a neutrino interpretation would be quite natural. Moreover, such nonstandard neutrino interactions are rather weakly constrained and could well produce sizeable $j + \text{MET}$ rates at the LHC. Here we investigated two useful tools that may aid in this discrimination: $\not{E}_T$ shape analysis of monojet data and multilepton data.

We found that NSI can be discriminated from DM based on $\not{E}_T$ shape analysis if the DM mass is $\gtrsim$1 TeV.

Next the $SU(2)$ charge of neutrinos implies that NSI contributes in channels involving charged leptons. This gives a simple discriminant between neutrino explanations of missing energy from singlet DM. To this end we studied $jj + \ell + \text{MET}$ and $\tau + e + \text{MET}$ events to derive new limits on NSI. We have found that NSI mediators with masses $\gtrsim$800 GeV can be fairly robustly discriminated from DM interpretations. This is because the above multilepton channels offer greater sensitivity at large mediator masses than monojets. In particular, for mediator masses greater than 1.5 TeV both channels are separately strong enough to discriminate between NSI and DM. Light mediator NSI remains hard to probe with LHC data, which underscores the importance of upcoming low-energy probes of NSI.

## ACKNOWLEDGMENTS

I. M. S. would like to thank the organizers of the *Santa Fe Summer Workshop, Implications of Neutrino Flavor Oscillations (INFO) 2015* and the $\nu$@*Fermilab* workshop for the opportunity to present this work. The CP$^3$-Origins Center is partially funded by the Danish National Research Foundation, Grant No. DNRF90.

[1] M. Cirelli, N. Fornengo, and A. Strumia, Minimal dark matter, Nucl. Phys. **B753**, 178 (2006).
[2] A. Birkedal, K. Matchev, and M. Perelstein, Dark matter at colliders: A Model independent approach, Phys. Rev. D **70**, 077701 (2004).
[3] Q.-H. Cao, C.-R. Chen, C. S. Li, and H. Zhang, Effective dark matter model: Relic density, CDMS II, Fermi LAT and LHC, J. High Energy Phys. 08 (2011) 018.
[4] M. Beltran, D. Hooper, E. W. Kolb, Z. A. C. Krusberg, and T. M. P. Tait, Maverick dark matter at colliders, J. High Energy Phys. 09 (2010) 037.
[5] J. Goodman, M. Ibe, A. Rajaraman, W. Shepherd, T. M. P. Tait, and H.-B. Yu, Constraints on light majorana dark matter from colliders, Phys. Lett. B **695**, 185 (2011).
[6] J. Goodman, M. Ibe, A. Rajaraman, W. Shepherd, T. M. P. Tait, and H.-B. Yu, Constraints on dark matter from colliders, Phys. Rev. D **82**, 116010 (2010).
[7] Y. Bai, P. J. Fox, and R. Harnik, The Tevatron at the frontier of dark matter direct detection, J. High Energy Phys. 12 (2010) 048.
[8] J.-F. Fortin and T. M. P. Tait, Collider Constraints on Dipole-Interacting Dark Matter, Phys. Rev. D **85**, 063506 (2012).
[9] M. L. Graesser, I. M. Shoemaker, and L. Vecchi, A dark force for baryons, arXiv:1107.2666.
[10] P. J. Fox, R. Harnik, J. Kopp, and Y. Tsai, Missing energy signatures of dark matter at the LHC, Phys. Rev. D **85**, 056011 (2012).
[11] A. Friedland, M. L. Graesser, I. M. Shoemaker, and L. Vecchi, Probing nonstandard standard model backgrounds with LHC monojets, Phys. Lett. B **714**, 267 (2012).
[12] I. M. Shoemaker and L. Vecchi, Unitarity and Monojet Bounds on Models for DAMA, CoGeNT, and CRESST-II, Phys. Rev. D **86**, 015023 (2012).
[13] H. An, X. Ji, and L.-T. Wang, Light dark matter and $Z'$ dark force at colliders, J. High Energy Phys. 07 (2012) 182.
[14] P. J. Fox, R. Harnik, R. Primulando, and C.-T. Yu, Taking a razor to dark matter parameter space at the LHC, Phys. Rev. D **86**, 015010 (2012).
[15] L. M. Carpenter, A. Nelson, C. Shimmin, T. M. Tait, and D. Whiteson, Collider searches for dark matter in events with a $Z$-boson and missing energy, Phys. Rev. D **87**, 074005 (2013).
[16] S. Chatrchyan *et al.* (CMS Collaboration), Search for Dark Matter and Large Extra Dimensions in pp Collisions Yielding a Photon and Missing Transverse Energy, Phys. Rev. Lett. **108**, 261803 (2012).
[17] M. T. Frandsen, F. Kahlhoefer, A. Preston, S. Sarkar, and K. Schmidt-Hoberg, LHC and Tevatron bounds on the dark matter direct detection cross-section for vector mediators, J. High Energy Phys. 07 (2012) 123.
[18] U. Haisch, F. Kahlhoefer, and J. Unwin, The impact of heavy-quark loops on LHC dark matter searches, J. High Energy Phys. 07 (2013) 125.
[19] N. F. Bell, J. B. Dent, A. J. Galea, T. D. Jacques, L. M. Krauss, and T. J. Weiler, Searching for dark matter at the LHC with a mono-Z, Phys. Rev. D **86**, 096011 (2012).
[20] P. J. Fox and C. Williams, Next-to-leading order predictions for dark matter production at hadron colliders, Phys. Rev. D **87**, 054030 (2013).
[21] N. Zhou, D. Berge, and D. Whiteson, Mono-everything: combined limits on dark matter production at colliders from multiple final states, Phys. Rev. D **87**, 095013 (2013).
[22] G. Busoni, A. De Simone, E. Morgante, and A. Riotto, On the validity of the effective field theory for dark matter searches at the LHC, Phys. Lett. B **728**, 412 (2014).
[23] H. An, L.-T. Wang, and H. Zhang, Dark matter with $t$-channel mediator: A simple step beyond contact interaction, Phys. Rev. D **89**, 115014 (2014).
[24] O. Buchmueller, M. J. Dolan, and C. McCabe, Beyond effective field theory for dark matter searches at the LHC, J. High Energy Phys. 01 (2014) 025.
[25] G. Busoni, A. De Simone, J. Gramling, E. Morgante, and A. Riotto, On the validity of the effective field theory for dark matter searches at the LHC, Part II: Complete analysis for the $s$-channel, J. Cosmol. Astropart. Phys. 06 (2014) 060.
[26] O. Buchmueller, M. J. Dolan, S. A. Malik, and C. McCabe, Characterising dark matter searches at colliders and direct detection experiments: Vector mediators, J. High Energy Phys. 01 (2015) 037.
[27] J. Abdallah *et al.*, Simplified models for dark matter and missing energy searches at the LHC, arXiv:1409.2893.
[28] T. Jacques and K. Nordström, Mapping monojet constraints onto simplified dark matter models, J. High Energy Phys. 06 (2015) 142.
[29] M. Chala, F. Kahlhoefer, M. McCullough, G. Nardini, and K. Schmidt-Hoberg, Constraining dark sectors with monojets and dijets, arXiv:1503.05916.
[30] N. F. Bell, Y. Cai, J. B. Dent, R. K. Leane, and T. J. Weiler, Dark matter at the LHC: EFTs and gauge invariance, arXiv:1503.0787.
[31] N. F. Bell, V. Cirigliano, M. J. Ramsey-Musolf, P. Vogel, and M. B. Wise, How magnetic is the Dirac neutrino?, Phys. Rev. Lett. **95**, 151802 (2005).
[32] A. Beda *et al.*, Upper limit on the neutrino magnetic moment from three years of data from the GEMMA spectrometer, arXiv:1005.2736.
[33] V. Barger, W.-Y. Keung, D. Marfatia, and P.-Y. Tseng, Dipole moment dark matter at the LHC, Phys. Lett. B **717**, 219 (2012).
[34] J. F. Beacom and P. Vogel, Neutrino magnetic moments, flavor mixing, and the Super-Kamiokande solar data, Phys. Rev. Lett. **83**, 5222 (1999).
[35] L. Wolfenstein, Neutrino oscillations in matter, Phys. Rev. D **17**, 2369 (1978).
[36] S. Davidson, C. Pena-Garay, N. Rius, and A. Santamaria, Present and future bounds on nonstandard neutrino interactions, J. High Energy Phys. 03 (2003) 011.
[37] A. Friedland, C. Lunardini, and C. Pena-Garay, Solar neutrinos as probes of neutrino matter interactions, Phys. Lett. B **594**, 347 (2004).
[38] A. Friedland, C. Lunardini, and M. Maltoni, Atmospheric neutrinos as probes of neutrino-matter interactions, Phys. Rev. D **70**, 111301 (2004).
[39] A. Friedland and C. Lunardini, A test of tau neutrino interactions with atmospheric neutrinos and K2K, Phys. Rev. D **72**, 053009 (2005).
[40] K. Scholberg, Prospects for measuring coherent neutrino-nucleus elastic scattering at a stopped-pion neutrino source, Phys. Rev. D **73**, 033005 (2006).

[41] A. Friedland and C. Lunardini, Two modes of searching for new neutrino interactions at MINOS, Phys. Rev. D **74**, 033012 (2006).

[42] J. Kopp, T. Ota, and W. Winter, Neutrino factory optimization for non-standard interactions, Phys. Rev. D **78**, 053007 (2008).

[43] J. Kopp, M. Lindner, T. Ota, and J. Sato, Non-standard neutrino interactions in reactor and superbeam experiments, Phys. Rev. D **77**, 013007 (2008).

[44] S. Davidson and V. Sanz, Non-standard neutrino interactions at colliders, Phys. Rev. D **84**, 113011 (2011).

[45] A. Friedland and I. M. Shoemaker, Searching for novel neutrino interactions at NOvA and beyond in light of large $\theta_{13}$, arXiv:1207.6642.

[46] I. Mocioiu and W. Wright, Non-standard neutrino interactions in the mu–tau sector, Nucl. Phys. **B893**, 376 (2015).

[47] M. B. Wise and Y. Zhang, Effective theory and simple completions for neutrino interactions, Phys. Rev. D **90**, 053005 (2014).

[48] A. Sousa (MINOS and MINOS+ Collaborations), First MINOS+ data and new results from MINOS, arXiv:1502.0771.

[49] T. Ohlsson, Status of non-standard neutrino interactions, Rep. Prog. Phys. **76**, 044201 (2013).

[50] O. G. Miranda and H. Nunokawa, Non standard neutrino interactions, arXiv:1505.06254.

[51] A. Bolanos, O. Miranda, A. Palazzo, M. Tortola, and J. Valle, Probing non-standard neutrino-electron interactions with solar and reactor neutrinos, Phys. Rev. D **79**, 113012 (2009).

[52] A. Palazzo and J. Valle, Confusing non-zero $\theta_{13}$ with non-standard interactions in the solar neutrino sector, Phys. Rev. D **80**, 091301 (2009).

[53] A. Palazzo, Hint of non-standard dynamics in solar neutrino conversion, Phys. Rev. D **83**, 101701 (2011).

[54] R. Bonventre, A. LaTorre, J. R. Klein, G. D. O. Gann, S. Seibert, and O. Wasalski, Non-Standard Models, Solar Neutrinos, and Large $\theta_{13}$, Phys. Rev. D **88**, 053010 (2013).

[55] M. Gonzalez-Garcia and M. Maltoni, Determination of matter potential from global analysis of neutrino oscillation data, J. High Energy Phys. 09 (2013) 152.

[56] Y. Farzan, A model for large non-standard interactions of neutrinos leading to the LMA-Dark solution, arXiv:1505.06906.

[57] M. Maltoni and A. Yu. Smirnov, Solar neutrinos and neutrino physics, Eur. Phys. J. A **52**, 87 (2016).

[58] N. Fornengo, M. Maltoni, R. Tomas, and J. Valle, Probing neutrino nonstandard interactions with atmospheric neutrino data, Phys. Rev. D **65**, 013010 (2001).

[59] M. M. Guzzo, P. C. de Holanda, M. Maltoni, H. Nunokawa, M. A. Tórtola, and J. W. F. Valle, Status of a hybrid three neutrino interpretation of neutrino data, Nucl. Phys. **B629**, 479 (2002).

[60] M. Gonzalez-Garcia and M. Maltoni, Atmospheric neutrino oscillations and new physics, Phys. Rev. D **70**, 033010 (2004).

[61] M. Gonzalez-Garcia, M. Maltoni, and J. Salvado, Testing matter effects in propagation of atmospheric and long-baseline neutrinos, J. High Energy Phys. 05 (2011) 075.

[62] J. A. B. Coelho, T. Kafka, W. A. Mann, J. Schneps, and O. Altinok, Constraints for non-standard interaction $\epsilon\_e\tau V\_e$ from $\nu\_e$ appearance in MINOS and T2K, Phys. Rev. D **86**, 113015 (2012).

[63] Z. Berezhiani and A. Rossi, Limits on the nonstandard interactions of neutrinos from $e + e-$ colliders, Phys. Lett. B **535**, 207 (2002).

[64] G. Mangano, G. Miele, S. Pastor, T. Pinto, O. Pisanti, and P. D. Serpico, Effects of non-standard neutrino-electron interactions on relic neutrino decoupling, Nucl. Phys. **B756**, 100 (2006).

[65] S. Bergmann, Y. Grossman, and D. M. Pierce, Can lepton flavor violating interactions explain the atmospheric neutrino problem?, Phys. Rev. D **61**, 053005 (2000).

[66] S. Bergmann, M. Guzzo, P. de Holanda, P. Krastev, and H. Nunokawa, Status of the solution to the solar neutrino problem based on nonstandard neutrino interactions, Phys. Rev. D **62**, 073001 (2000).

[67] C. Degrande, C. Duhr, B. Fuks, D. Grellscheid, O. Mattelaer, and T. Reiter, UFO—The Universal FeynRules Output, Comput. Phys. Commun. **183**, 1201 (2012).

[68] S. Antusch, J. P. Baumann, and E. Fernandez-Martinez, Non-standard neutrino interactions with matter from physics beyond the standard model, Nucl. Phys. **B810**, 369 (2009).

[69] M. Gavela, D. Hernandez, T. Ota, and W. Winter, Large gauge invariant non-standard neutrino interactions, Phys. Rev. D **79**, 013007 (2009).

[70] Y. Farzan and I. M. Shoemaker, Lepton flavor violating non-standard interactions via light mediators, Phys. Rev. D **79**, 013007 (2009).

[71] P. J. Fox, J. Liu, D. Tucker-Smith, and N. Weiner, An Effective Z', Phys. Rev. D **84**, 115006 (2011).

[72] P. Gondolo, P. Ko, and Y. Omura, Light dark matter in leptophobic Z' models, Phys. Rev. D **85**, 035022 (2012).

[73] T. Lin, H.-B. Yu, and K. M. Zurek, On symmetric and asymmetric light dark matter, Phys. Rev. D **85**, 063503 (2012).

[74] H. An, R. Huo, and L.-T. Wang, Searching for Low Mass Dark Portal at the LHC, Phys. Dark Univ. **2**, 50 (2013).

[75] A. Alves, S. Profumo, and F. S. Queiroz, The dark $Z'$ portal: direct, indirect and collider searches, J. High Energy Phys. 04 (2014) 063.

[76] G. Arcadi, Y. Mambrini, M. H. G. Tytgat, and B. Zaldivar, Invisible $Z'$ and dark matter: LHC vs LUX constraints, J. High Energy Phys. 03 (2014) 134.

[77] O. Lebedev and Y. Mambrini, Axial dark matter: The case for an invisible $Z'$, Phys. Lett. B **734**, 350 (2014).

[78] S. Davidson, Including the Z in an Effective Field Theory for dark matter at the LHC, J. High Energy Phys. 10 (2014) 84.

[79] M. Fairbairn and J. Heal, Complementarity of dark matter searches at resonance, Phys. Rev. D **90**, 115019 (2014).

[80] D. E. Soper, M. Spannowsky, C. J. Wallace, and T. M. P. Tait, Scattering of dark particles with light mediators, Phys. Rev. D **90**, 115005 (2014).

[81] D. Hooper, $Z'$ mediated dark matter models for the Galactic Center gamma-ray excess, Phys. Rev. D **91**, 035025 (2015).

[82] J. Alwall, R. Frederix, S. Frixione, V. Hirschi, F. Maltoni, O. Mattelaer, H.-S. Shao, T. Stelzer, P. Torrielli, and M. Zaro, The automated computation of tree-level and next-to-leading order differential cross sections, and their matching to parton shower simulations, J. High Energy Phys. 07 (2014) 079.

[83] P. de Aquino, W. Link, F. Maltoni, O. Mattelaer, and T. Stelzer, ALOHA: Automatic Libraries Of Helicity Amplitudes for Feynman diagram computations, Comput. Phys. Commun. **183**, 2254 (2012).

[84] T. Sjostrand, S. Mrenna, and P. Z. Skands, PYTHIA 6.4 physics and manual, J. High Energy Phys. 05 (2006) 026.

[85] T. Sjostrand, S. Mrenna, and P. Z. Skands, A brief introduction to PYTHIA 8.1, Comput. Phys. Commun. **178**, 852 (2008).

[86] J. S. Conway *et al.*, http://www.physics.ucdavis.edu/conway/research/software/pgs/pgs4-general.htm.

[87] J. de Favereau, C. Delaere, P. Demin, A. Giammanco, V. Lemaître, A. Mertens, and M. Selvaggi (DELPHES 3 Collaboration), DELPHES 3, A modular framework for fast simulation of a generic collider experiment, J. High Energy Phys. 02 (2014) 057.

[88] J. Pumplin, D. R. Stump, J. Huston, H. L. Lai, P. M. Nadolsky, and W. K. Tung, New generation of parton distributions with uncertainties from global QCD analysis, J. High Energy Phys. 07 (2002) 012.

[89] R. D. Ball *et al.*, Parton distributions with LHC data, Nucl. Phys. **B867**, 244 (2013).

[90] CMS Collaboration, Search for new physics in monojet events in pp collisions at $sqrt(s) = 8$ TeV, CMS-PAS-EXO-12-048.

[91] M. L. Mangano, M. Moretti, F. Piccinini, and M. Treccani, Matching matrix elements and shower evolution for top-quark production in hadronic collisions, J. High Energy Phys. 01 (2007) 013.

[92] G. Aad *et al.* (ATLAS Collaboration), Search for supersymmetry in events with large missing transverse momentum, jets, and at least one tau lepton in 20 $\text{fb}^{-1}$ of $\sqrt{s} = 8$ TeV proton-proton collision data with the ATLAS detector, J. High Energy Phys. 09 (2014) 103.

[93] G. Aad *et al.* (ATLAS Collaboration), Search for production of $WW/WZ$ resonances decaying to a lepton, neutrino and jets in $pp$ collisions at $\sqrt{s} = 8$ TeV with the ATLAS detector, J. High Energy Phys. 09 (2014) 103.

[94] M. Cacciari, G. P. Salam, and G. Soyez, FastJet user manual, Eur. Phys. J. C **72**, 1896 (2012).

[95] U. Baur, T. Han, and J. Ohnemus, $WZ$ production at hadron colliders: Effects of nonstandard $WWZ$ couplings and QCD corrections, Phys. Rev. D **51**, 3381 (1995).

[96] E. Accomando, A. Belyaev, L. Fedeli, S. F. King, and C. Shepherd-Themistocleous, Z' physics with early LHC data, Phys. Rev. D **83**, 075012 (2011).

[97] G. P. Zeller *et al.* (NuTeV Collaboration), A Precise Determination of Electroweak Parameters in Neutrino Nucleon Scattering, Phys. Rev. Lett. **88**, 091802 (2002); [Phys. Rev. Lett. **90**, 239902 (2003).

[98] J. Dorenbosch *et al.* (CHARM Collaboration), Experimental verification of the universality of $\nu\_e$ and $\nu\_\mu$ coupling to the neutral weak current, Phys. Lett. B **180**, 303 (1986).

[99] M. Drees and C.-L. Shan, Model-independent determination of the WIMP mass from direct dark matter detection data, J. Cosmol. Astropart. Phys. 06 (2008) 012.

[100] S. D. McDermott, H.-B. Yu, and K. M. Zurek, The dark matter inverse problem: Extracting particle physics from scattering events, Phys. Rev. D **85**, 123507 (2012).

[101] J. F. Cherry, M. T. Frandsen, and I. M. Shoemaker, Halo independent direct detection of momentum-dependent dark matter, J. Cosmol. Astropart. Phys. 10 (2014) 022.

[102] A. Bolozdynya *et al.*, Opportunities for neutrino physics at the spallation neutron source: A white paper, arXiv:1211.5199.

[103] D. Akimov *et al.* (CSI Collaboration), Community Summer Study 2013: Snowmass on the Mississippi (CSS2013) Minneapolis, MN, 2013 (unpublished).

[104] J. Billard, L. Strigari, and E. Figueroa-Feliciano, Solar neutrino physics with low-threshold dark matter detectors, Phys. Rev. D **91**, 095023 (2015).